ARTICLE

Mutations in LOXHD1, an Evolutionarily Conserved Stereociliary Protein, Disrupt Hair Cell Function in Mice and Cause Progressive Hearing Loss in Humans

Nicolas Grillet,[1,11] Martin Schwander,[1,11] Michael S. Hildebrand,[2] Anna Sczaniecka,[1] Anand Kolatkar,[1] Janice Velasco,[3] Jennifer A. Webster,[4] Kimia Kahrizi,[5] Hossein Najmabadi,[5] William J. Kimberling,[6] Dietrich Stephan,[3,7,8] Melanie Bahlo,[9] Tim Wiltshire,[10] Lisa M. Tarantino,[10] Peter Kuhn,[1] Richard J.H. Smith,[2] and Ulrich Müller[1,*]

Hearing loss is the most common form of sensory impairment in humans and is frequently progressive in nature. Here we link a previously uncharacterized gene to hearing impairment in mice and humans. We show that hearing loss in the ethylnitrosourea (ENU)-induced *samba* mouse line is caused by a mutation in *Loxhd1*. LOXHD1 consists entirely of PLAT (polycystin/lipoxygenase/α-toxin) domains and is expressed along the membrane of mature hair cell stereocilia. Stereociliary development is unaffected in *samba* mice, but hair cell function is perturbed and hair cells eventually degenerate. Based on the studies in mice, we screened DNA from human families segregating deafness and identified a mutation in *LOXHD1*, which causes DFNB77, a progressive form of autosomal-recessive nonsyndromic hearing loss (ARNSHL). *LOXHD1*, *MYO3a,* and *PJVK* are the only human genes to date linked to progressive ARNSHL. These three genes are required for hair cell function, suggesting that age-dependent hair cell failure is a common mechanism for progressive ARNSHL.

Introduction

Hearing impairment in humans is frequently genetic in origin and progressive in nature. Genetic transmission is recessive in ~80% of cases and dominant in ~15%–18%, with X-linked and mitochondrial inheritance making small fractional contributions.[1,2] The identified genes encode proteins with diverse functions, including transcription factors, cell adhesion molecules, and ion channels. Interestingly, most mutations that segregate with recessive hearing loss cause congenital deafness that is nonprogressive, whereas mutations segregating with dominant hearing loss typically lead to postlingual progressive hearing loss.[1] Age-related hearing loss, known as presbycusis, also shows a genetic predisposition with onset and progression reflecting complex interactions between genetic and environmental factors.[3,4] Although substantial progress has been made in determining cellular functions disrupted in congenital nonprogressive deafness, comparatively little is known about the mechanisms that underlie progressive postlingual hearing loss.

To identify genetic defects that cause auditory impairment, several laboratories have studied mouse models carrying naturally occurring or ENU-induced mutations that cause hearing loss. The structural and functional similarity of the murine and human auditory systems has validated this approach, with innumerable examples of orthologous genes in these species causing comparable phenotypes.[5–9] However, examples of genetic mutations that lead to progressive autosomal-recessive nonsyndromic hearing loss (ARNSHL) are extremely rare. Included in this list are mutations in the genes encoding the cytoplasmic protein pejvakin (PJVK) and the cadherin superfamily member cadherin 23 (CDH23), which lead to progressive hearing loss in mice.[10,11] Mutations in *PJVK* also segregate with progressive ARNSHL in humans (DFNB59 [MIM 610219]),[10] as do mutations in *MYO3A* (DFNB30 [MIM 606808]).[12,13] All of these genes are expressed in hair cells, suggesting that intrinsic defects of hair cell function may be common to progressive ARNSHL. In contrast, nonprogressive ARNSHL that is profound is typically associated with severe hair cell damage, or in cases of more moderate hearing loss, damage to supporting structures like the tectorial membrane in *TECTA*-associated hearing loss (DFNA8, DFNA12, DFNB21 [MIM 602574]).[1]

We describe here the identification of a recessive mutation in the *samba* mouse line, which we generated in an ENU-mutagenesis screen.[10] The *samba* mutation introduces a missense mutation in the previously uncharacterized *Loxhd1* gene and leads to congenital deafness. Its human ortholog represents a previously not known ARNSHL locus, DFNB77, which maps to chromosome 18q12-q21 (35–56 Mb). The segregating nonsense mutation in *LOXHD1* is predicted to introduce a premature stop codon

[1]Department of Cell Biology, The Scripps Research Institute, La Jolla, CA 92037, USA; [2]Department of Otolaryngology—Head and Neck Surgery, University of Iowa City, IA 55242, USA; [3]Genome Institute of the Novartis Research Foundation, San Diego, CA 92121, USA; [4]Neurogenomics Division, Translational Genomics Research Institute, Phoenix, AZ 85004, USA; [5]Genetics Research Center, University of Social Welfare and Rehabilitation Sciences, Tehran, Iran; [6]Department of Genetics, Boys Town National Research Hospital, Omaha, NE 68131, USA; [7]Arizona Alzheimer's Consortium, Phoenix, AZ 85004, USA; [8]Banner Alzheimer's Institute, Phoenix, AZ 85004, USA; [9]Bioinformatics Division, The Walter and Eliza Hall Institute of Medical Research, Parkville 3052 VIC, Australia; [10]Department of Psychiatry, University of North Carolina, Chapel Hill, NC 27516, USA
[11]These authors contributed equally to this work
*Correspondence: umueller@scripps.edu
DOI 10.1016/j.ajhg.2009.07.017.

and leads to progressive ARNSHL, suggesting that different mutations in LOXHD1 lead to distinct disease phenotypes. The human and murine LOXHD1 proteins consist of 15 PLAT (polycystin/lipoxygenase/α-toxin) domains, which share structural similarity to eukaryotic Ca^{2+}-binding C2 domains.[14] PLAT domains are believed to be involved in targeting of proteins to the plasma membrane.[15,16] Consistent with this model, LOXHD1 is localized in hair cells along the plasma membrane of stereocilia. Although stereociliary development is unaffected in *samba* mice, hair cells show functional defects and eventually degenerate. *LOXHD1* therefore joins *PJVK* and *MYO3A* as a gene associated with progressive ARNSHL and further supports the hypothesis that defects in hair cell function are responsible for this type of progressive hearing loss.

Material and Methods

Ethic Statement

Human Research Institutional Review Boards at the Welfare Science and Rehabilitation University and the Iran University of Medical Sciences, Tehran, Iran, and the University of Iowa, Iowa City, Iowa, USA approved all procedures. IACUC Institutional Review Boards at the Scripps Research Institute, La Jolla, California, USA approved all animal procedures.

ABR and DPOAE Measurement and Mapping of the *Samba* Mutation

ABR and DPOAE measurements, vestibular function tests, and SNP mapping were carried out as described.[10] To identify the *samba* mutation, a list of annotated genes in the affected interval was established with the UCSC genome browser. The affected genomic region was also compared across species to identify conserved regions that might encode additional genes. RNA was prepared from the inner ear of P7 wild-type and *samba* mice, retrotranscribed with MMLV-RT, and amplified by RT-PCR with random primers and JumpStart Accu Taq LA DNA polymerase (Sigma). Primers were designed for the sequencing of annotated and predicted genes (Table S1 available online).

Histology, Electron Microscopy, and Immunolocalization Studies

Staining of histological sections and scanning electron microscopy were carried out as described.[10,26] For immunolocalization studies, we raised antibodies against LOXHD1. Rabbits were coinjected with two synthetic peptides derived from the sequence of PLAT domains 11 and 12 (VTTGKHKEAATDSRAF, NGSTEEVQLD KKKARFEREQND). The peptide sequences show no homology with any other protein in publically available databases. To assess antibody specificity, we transfected NIH 3T3 cells with an expression vector (pEGFP-C3, Clontech) encoding PLAT domains 8–15 of LOXHD1 fused to EGFP. Protein expression was evaluated by western blotting and immunofluorescence analysis with purified LOXHD1 antibody as described.[26] Cochlear whole-mount staining was carried out as described.[26] For peptide competition experiment, the LOXHD1 antibody was incubated for 30 min at RT with the LOXHD1 peptides (50 μg/ml) or unrelated peptide and then used for whole-mount immunostaining. For immunogold localization, animals were perfused with 4% PFA, 0.025% glutaraldehyde in Na-cacodylate 0.1 M (pH 7.4), 0.025% picric acid. The cochlear shell was opened and incubated in the same fixative for 1 hr. Tissue was washed with Tris-buffered saline (TBS, 150 mM NaCl, 10 mM Tris-HCl; pH 7.6), and the cochlear shell, Reissner's membrane, and tectorial membrane were removed. Tissue was blocked for 1 hr at room temperature in TBS containing 4% BSA and 0.02% Triton X-100 and incubated overnight at 4°C with LOXHD1 antibody in TBS containing 1% BSA and 0.02% Triton X-100. Tissue was washed in TBS and incubated for 2 days at 4°C with anti-rabbit antibody conjugated with colloidal gold beads. Tissue was washed in TBS and 0.1 M Na-cacodylate and postfixed for 24 hr at 4°C with 2.5% glutaraldehyde in 0.1 M Na-cacodylate. Decalcification of the modiolus was performed by adding 1:3 Vol/Vol 0.5 M EDTA (pH 8.0) to fixative and incubation for 3 hr at 4°C. Tissue was washed with 0.1 M Na-cacodylate and postfixed for 1.5 hr in 1% OsO_4 in 0.1 M Na-Cacodylate, washed, dehydrated, and cleared in propylene oxide. Tissue was impregnated in Epon/Araldite resin and the organ of Corti further microdissected and samples polymerized at 60°C. Thick sections were initially taken to assess the orientation. Thin sections were cut and poststained for 30 min with uranyl acetate followed by 20 min incubation in lead citrate. Grids were examined on a Philips CM100 electron microscope (FEI, Hillsbrough, OR). Images were documented with Kodak S0163 EM film. Negatives were scanned at 605 Ipi with a Fuji FineScan 2750xl (Hemel, Hempstead, Herts, UK).

In Situ Hybridization

The LOXHD1 mRNA (GenBank FJ50876) was amplified from the murine P7 cochlea with Phusion (New England Biolabs) and cloned into pGEM-T (Promega). 5′ and 3′ in situ probes were generated from LOXHD1 cDNAs cloned from P7 organ of Corti (with the following primers: 5′: CAGAAGAAGAAGCGGAGGAAG AAAGAC and TACGCTCGCCTGTGTCTCCATACTCTC [0.6 Kb]; 3′: CCCTCCTGAAGTCCTCCAAAACCA and ACACCCTGCAGCA AGTCCCAACC [3.6 Kb]). In situ hybridization was carried out as described.[10]

Molecular Modeling

With Modeler (version 9v6),[27] the mouse PLAT10 domain sequence was threaded onto the PLAT domain of (chain A; PDB ID, 2FNQ) allene oxide synthase-lipoxygenase protein via the automodel class and the sequence alignment produced by ClustalW.[28] This model was energy minimized to remove bad contacts. The minimized, threaded coordinates were used to mutate Ile88 to Asn and produce a mutant model that was energy minimized. Minimization consisted of 20 cycles of conjugate gradient minimization followed by 50 cycles of molecular dynamics optimization with the Verlet algorithm at 300K and finished with 100 cycles of conjugate gradient minimization.

Family Report, SNP Genotyping, and Linkage Analysis

A five-generation consanguineous Iranian family segregating postlingual ARNSHL was investigated. On consenting persons, audiologic testing was completed and a physical examination was performed to exclude clinical features consistent with syndromic hearing loss. The hearing status of individuals III-1 and III-2 was reportedly normal although hearing tests were not conducted. Age of death for these individuals was unavailable. Ten milliliters of whole blood were obtained as a DNA source. Genomic DNA from individuals IV:1, IV:2, V:1, V:4, V:5, V:6, V:7, V:8, and V:9 was genotyped for 50,000 SNPs via the Affymetrix 50K XBA

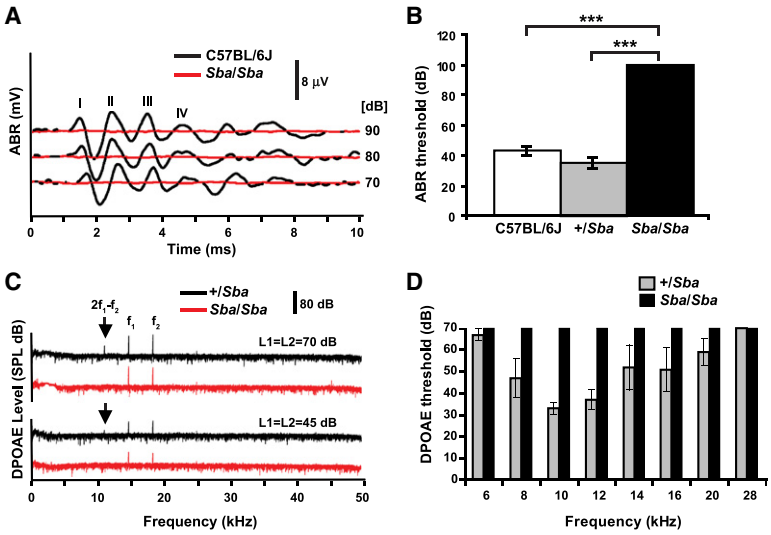

Figure 1. Auditory Defects in *samba* Mice at 3 Weeks of Age

(A) Representative click-evoked ABRs for wild-type (C57Bl6/J) mice and homozygous *samba* mutants at different sound intensities. ABR peaks I-IV are indicated. *samba* mutants showed no response even at the highest sound intensity (90 dB).

(B) Average auditory thresholds in 3-week-old mice (C57Bl/6J, n = 5; $Sba^{+/-}$, n = 4; $Sba^{-/-}$, n = 6; mean ± SD; ***$p < 0.001$, Student's t test).

(C) Representative DPOAE response spectra from a 3-week-old wild-type and homozygous *samba* mouse at a single stimulus condition (median primary frequency = 16 kHz). The cubic distortion product ($2f_1$-f_2) was absent in the mutants (black arrow).

(D) DPOAE thresholds in 3-week-old *samba* mutants were elevated at all frequencies analyzed (wild-type, n = 4; *samba*, n = 6; mean ± SD). Primary frequencies were maintained at an f_2/f_1 ratio of 1.22 and L_1 was equal to L_2.

GeneChips (TGEN, Phoenix, AZ). Genotypes were determined via the BRLMM genotyping algorithm.[29,30] Genotyping data were examined with PEDSTATS[31] for Mendelian inheritance errors and with MERLIN[32] for errors based on inferred double recombination events between tightly linked markers. An autosomal, genome-wide parametric linkage analysis was performed because males and females appeared equally affected. All linkage analysis was performed with MERLIN via an abridged pedigree with the inbreeding loop that included individuals IV:1 and IV:2; the inbreeding loop involving III:1 and III:2 was excluded. The abridged pedigree had 18 bits and could be analyzed via exact multipoint linkage analysis.[32] A subset of 6432 single-nucleotide polymorphisms (SNPs) spaced approximately 0.5 cM apart across the genome and with an average heterozygosity of 0.43 was chosen from the 50K XBA set to satisfy the linkage equilibrium requirements of the Lander-Green algorithm.[33] Selection and assembly of the data were performed with an in-house PERL script. An initial parametric linkage analysis was run assuming a fully penetrant autosomal-recessive model with a disease allele frequency of Pr(a) = 0.0001 and penetrances of pr(disease|aa) = 1 = pr(disease|aA), Pr(disease|AA) = 0. Haplotypes inferred with Merlin were imported into Haplopainter.[34]

PCR and Sequencing

The *LOXHD1* gene was amplified with gene-specific primers (Table S2). Amplification reactions were cycled with a standard protocol on a GeneMate Genius thermocycler (ISC BioExpress, UT). Bidirectional sequencing of all exons and flanking regions was completed with BigDye v3.1 Terminator Cycle Sequencing Kit (Applied Biosystems, CA), according to the manufacturer's instructions. Sequencing products were resolved with an ABI 3730s Sequencer (Perkin Elmer, MA). All sequencing chromatograms were compared to published cDNA sequence; nucleotide changes were detected with Sequencher v4.5 (Gene Code Corporation, MI).

Results

Hearing Loss and Defects in Outer Hair Cell Function in *samba* Mice

To generate murine models of autosomal-recessive hearing loss and to facilitate the discovery of the underlying genetic mutations, we carried out an ENU mutagenesis screen.[10] The homozygotes of one such line, which we named *samba* (*Sba*), were noted to be deaf at 8 weeks of age; no other neurological abnormalities were observed and in particular vestibular function was intact.[10]

Auditory brainstem responses (ABRs) demonstrated that homozygous *samba* mice were hearing impaired by 3 weeks of age (Figures 1A and 1B; Figure S1). Heterozygous *samba* mice were not affected, demonstrating that the mutation was inherited as a recessive trait (Figure 1B). Distortion product otoacoustic emissions (DPOAEs), sounds emitted from the ear canal in response to stimulation by two phase-locked tones of different frequency, were absent in 3-week-old *samba* homozygotes at all frequencies tested (Figures 1C and 1D). These emissions depend on the mechanical activity of outer hair cells (OHCs), so the deafness in *samba* mice must be due, at least in part, to defects in OHC function.

samba Mice Carry a Missense Mutation in the *Loxhd1* Gene

To identify the affected gene, we crossed *samba* mice with BALB/cByJ and 129S1/SvlmJ mice, intercrossed the F1 offspring, and performed ABR tests and single-nucleotide polymorphism (SNP) mapping on F2 progeny (198 meiotic events). After mapping the affected locus to chromosomal position 18qE3 (75–77 Mb) (Figures 2A and 2B), we designed primers for all annotated (n = 14) and in silico predicted (n = 5) genes in the interval, amplified the corresponding mRNAs from the P7 organ of Corti, and directly sequenced the amplicons; for some genes, we also sequenced exons and exon-intron borders via genomic DNA (Table S1). We detected only one mutation in the previously uncharacterized *Loxhd1* (lipoxygenase homology domains 1) gene (Table S1).

Several cDNAs encoding part of *Loxhd1* have previously been cloned from testis and placenta (Figure S2), but the *Loxhd1* gene structure has not been fully explored. Based on sequence conservation between human and mice, we predict that *Loxhd1* contains 43 exons, which are

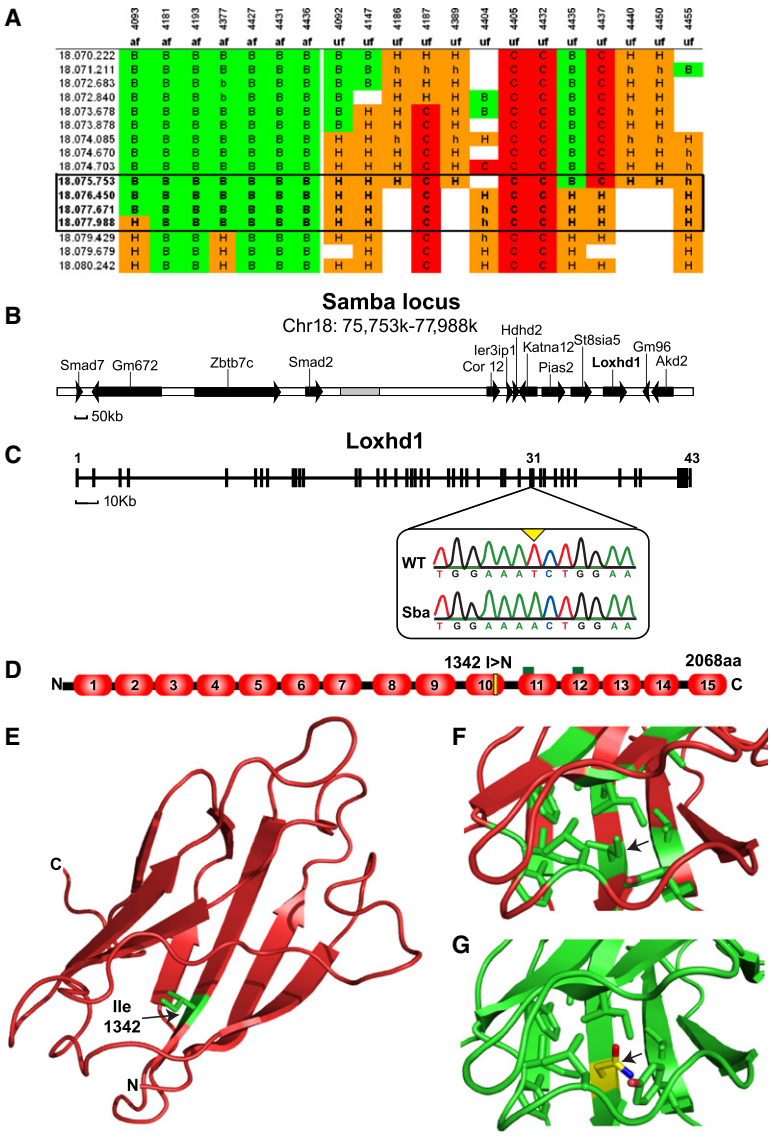

Figure 2. *samba* Mice Carry a Missense Mutation in *Loxhd1*

(A) DNA from affected (af) and unaffected (uf) mice was analyzed for SNP markers on chromosome 18, which are listed in the first column (the megabase position 70.222–80.242 is indicated). The mouse identification number and phenotypes are shown in the two top rows. The genotype for each marker is given as: B, homozygous C57Bl/6J; C, homozygous 129; H, heterozygous. The chromosomal interval that segregates with the mutant phenotype is highlighted in the box.

(B) The annotated genes in the affected interval in *samba* mice on chromosome 18 are indicated.

(C) Predicted exon/intron structure of the *Loxhd1* gene. Exons are shown as black squares. Several exons are numbered. The sequence chromatogram shows the mutation in exon 31.

(D) The LOXHD1 protein is predicted to consist of 15 PLAT domains. The samba mutation (1342 I>N) is indicated by a yellow bar, and the locations of the immunization peptides by green bars.

(E) Diagram of the PLAT 10 wild-type model. The cartoon is based on the C-alpha positions of the PLAT 10 model, which was derived from the PLAT domain of the allene oxide synthase-lipoxygenase coordinates (PDB ID: 2FNQ). The structure shows the characteristic two sheets of four β strands. The Ile1342 mutated in the *samba* mouse is highlighted in green.

(F) Diagram of the Ile1342 region of the wild-type PLAT 10 model. The ten side chains closest to the Ile are shown as sticks; carbon on the side chains is colored as green and oxygen as red. The Ile is seen to extend toward the opposing β-sheet and is surrounded by nine hydrophobic side chains. The nearest tyrosine presents the phenyl ring toward the hydrophobic pocket (arrow).

(G) Cartoon diagram of the Ile→Asn PLAT 10 mutant model in the hydrophobic pocket. The ten side chains closest to the Ile are shown as sticks; carbon on the side chains is colored as green, oxygen as red, and nitrogen as blue. The Asn side chain is predicted to extend into the hydrophobic cavity and is likely to destabilize the β sandwich.

distributed over 160 kB of genomic DNA (Figure S2). We succeeded in amplifying from the organ of Corti a cDNA containing 39 of the 42 coding exons, indicative of alternative splicing (Figure S2). The inner ear cDNA encodes a protein of 2068 amino acids and 15 PLAT (polycystin/lipoxygenase/α-toxin) domains (Figures 2C and 2D; Figure S2). We identified a T>A change (c.4025T>A) in the predicted coding sequence of *Loxhd1* (p.1342I>N) (Figures 2C and 2D; Figure S2; GenBank FJ50876). At the genomic level, this mutation was present in both *Loxhd1* alleles of *samba* mice (data not shown).

LOXHD1 is the first reported protein that consists entirely of PLAT domains. We identified conserved orthologs in vertebrates, cephalochordates (amphioxus: 45% identity, 64% similarity), and urochordates (ciona intestinalis: 41% identity, 60% similarity), but not in arthropods (*D. melanogaster*) or nematode (*C. elegans*) (Figures S3 and S4A; data not shown). A single PLAT domain consists of 120 amino acids and is present in proteins of diverse functions such as lipoxygenases, pancreatic lipase, the Rab6-interacting protein 1, and α-toxin of *Clostridium perfringens*.[17–20] The PLAT domain of the TRPP1/Polycystin-1 protein family[15] shows the highest homology to the PLAT domains in LOXHD1 (Figures S4B and S4C). Available data suggest that PLAT domains are important for targeting of these proteins to the plasma membrane.[15]

Each PLAT domain forms a β sandwich consisting of two sheets, each of four strands.[14,17,18,20] The *samba* mutation affects the tenth of 15 PLAT domains, converting a conserved isoleucine of the PLAT consensus sequence at position 1342 into an asparagine (Figure 2E; Figure S4B). Molecular threading of this mutation predicts that the substitution of a hydrophobic by a polar side chain in the highly hydrophobic cavity between the β sheets will destabilize the β sandwich structure (Figures 2F and 2G).

Loxhd1 Is Expressed in Hair Cells

By in situ hybridization, we observed *Loxhd1* expression in the developing inner ear at E13.5 and E16 but not in any other tissue (data not shown). At postnatal (P) day 4,

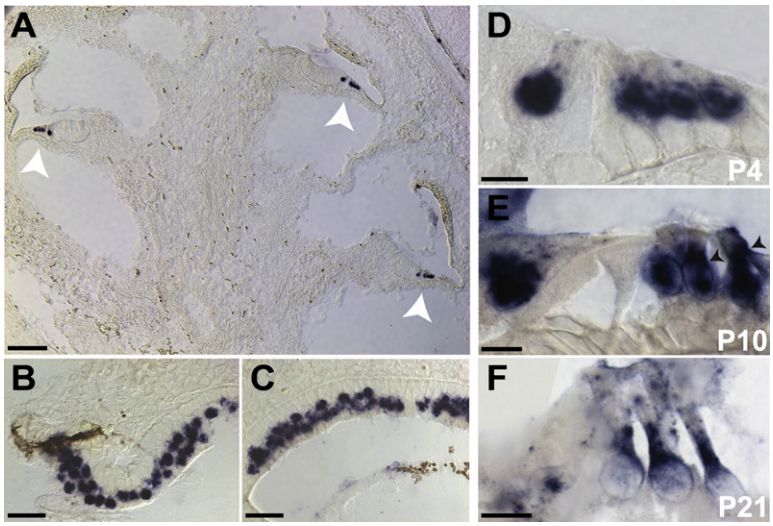

Figure 3. Analysis of *Loxhd1* Expression by In Situ Hybridization

(A–C) At P4, *Loxhd1* was specifically detected in cochlear hair cells (white arrows in A) and in vestibular hair cells (B, crista; C, saccule).

(D–F) The *Loxhd1* in situ hybridization signal was largely localized to the nucleus of P4 cochlear hair cells (D), over the nucleus and in the cytoplasm by P10 (E), and predominantly in the cytoplasm by P21 (F).

Scale bars represent 100 μm in (A), 20 μm in (B) and (C), and 10 μm in (D)–(F).

cochlear and vestibular hair cells were strongly positive for *Loxhd1* (Figures 3A–3D); no signal was observed with a control sense probe (data not shown). At this age, the transcript was highly concentrated in the nucleus or at its periphery (Figure 3D). By P10, staining was still observed in or around the nucleus but was also pronounced in the cytoplasm (Figure 3E); by P21, staining was prominent in the cytoplasm (Figure 3F). We obtained similar staining results with probes corresponding to the 5′ or 3′ parts of the mRNA (Figure S5). We therefore conclude that *Loxhd1* is expressed in the inner ear specifically in hair cells. Expression was maintained in *samba* mice (Figure S5), suggesting that mRNA stability was not significantly affected by the mutation.

To define the protein expression pattern of LOXHD1, we generated a rabbit polyclonal antibody against PLAT domains 11 and 12 (Figure 2D; Figure S3) that specifically detected LOXHD1 when expressed in heterologous cells (Figures S6A and S6B). In whole mounts, the antibody weakly stained at P2 the boundaries between hair and supporting cells, as well as hair cell stereocilia (Figures 4A and 4B). Staining of the hair-supporting cell boundary was no longer detectable by P10, although stereociliary staining was strong and remained so into adulthood (Figures 4C–4E). Staining was blocked by the immunogen peptide, further confirming the specificity of our antibody (Figure S6C).

LOXHD1 expression was also detected in stereocilia of vestibular hair cells, but the immunofluorescence signal was substantially less intense than in the cochlea (Figure 4F; Figure S6C). Staining of histological sections confirmed expression of LOXHD1 in stereocilia without any noticeable signal elsewhere in hair cells in the cochlea (Figures 4G and 4H) and vestibule (Figures 4I and 4J). Immunogold localization studies corroborated the immunofluorescence and demonstrated LOXHD1 localization along the length of stereocilia at the plasma membrane with the exception of their tips (Figure 4K). No signal was observed with preimmune serum or with secondary antibody alone (Figure 4B, and data not shown).

Defects in Hair Cell Morphology and Degeneration of Hair Cells and Spiral Ganglion Neurons

Histological analysis of inner ear morphology of P21 *samba* mutants failed to reveal obvious pathological changes (data not shown), and observations by scanning electron microscopy demonstrated the presence of three rows of OHCs and one row of inner hair cells (IHCs) with normally shaped stereociliary bundles (Figures 5A–5D; and data not shown). Inspection of hair cell ultrastructure in the apical and medial cochlear turns by transmission electron microscopy revealed normal stereociliary morphology, resolving a tapered lower end, the characteristic electron-dense tips, and the upper insertion site of the tip links (Figure 5K). No abnormalities in stereociliary width or in the space between the membrane and actin core of stereocilia were observed in the mutants (Figures 5P and 5Q).

The expressed mutant LOXHD1 protein in the *samba* cochlea correctly localized along the length of the stereocilia (Figures 5L–5Q).

Inspection of the basal turn of the cochlea was more revealing. By P21, some hair cells showed morphological defects, which manifested as fused stereocilia and membrane ruffling at the apical cell surface (Figures 5E–5J). Profound degenerative changes were obvious by P90 and included hair cell loss and a reduction in spiral ganglion neurons (Figures 5R–5Y; Figure S7). These data imply that the *samba* mutation leads to degenerative changes in the inner ear that are first observed in hair cells but subsequently affect other cell types including spiral ganglion neurons. Because *Loxhd1* is specifically expressed only in hair cells, degeneration of spiral ganglion neurons is likely a secondary consequence of perturbations in the function and maintenance of hair cells. Hearing function in *samba* mice is already affected at P21 (Figure 1; Figure S1), so structural defects in hair cells are likely a secondary consequence of functional defects.

A Premature Stop Codon in the Human *LOXHD1* Gene Causes Progressive ARNSHL

Based on our findings in mice, we searched for mutations in human families segregating ARNSHL. With genome-wide SNPs to complete linkage mapping, we identified a previously uncharacterized ARNSHL locus, DFNB77,

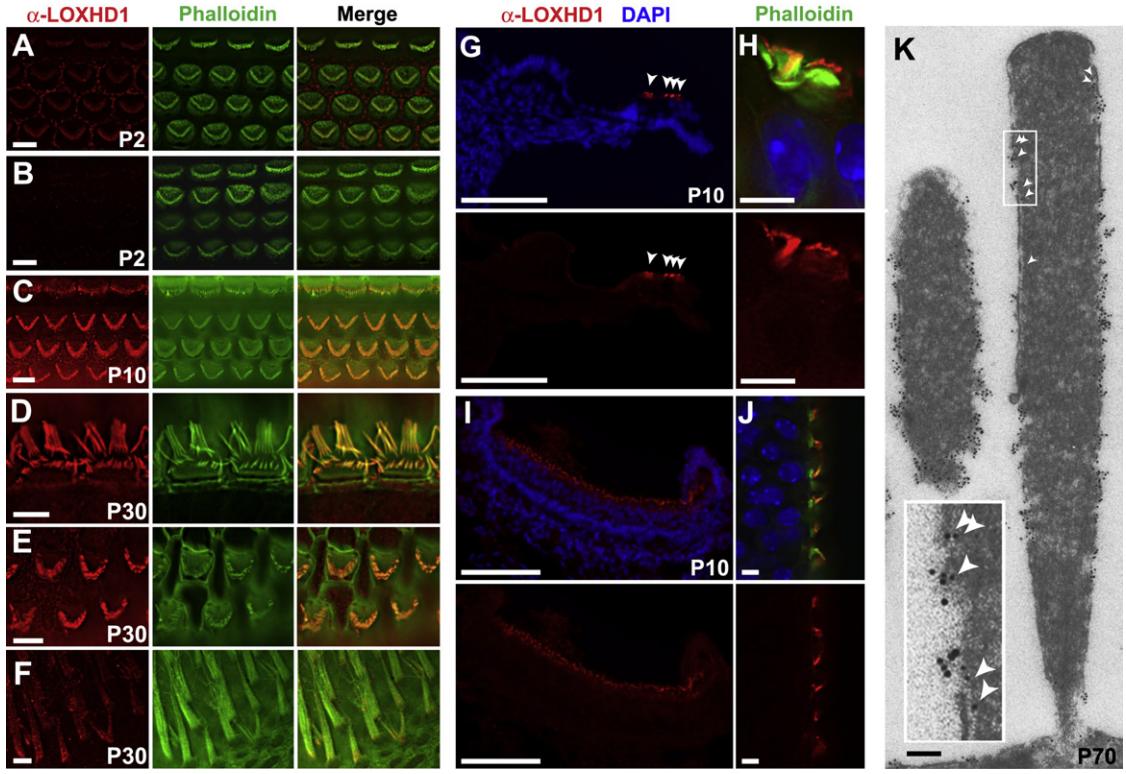

Figure 4. LOXHD1 Is Expressed in Hair Cells along the Length of Stereocilia
(A–F) Whole mounts of the cochlea (A–E) and cristae (F) at the indicated ages were stained with phalloidin (green) to reveal F-actin in stereocilia and with an antibody to LOXHD1 (red); in (B), preimmune serum was used instead of LOXHD1 antibody. LOXHD1 expression was weak at P2 and increases at subsequent ages. Expression remained high in hair cells from adult mice. Vestibular hair cells also expressed LOXHD1, but the fluorescence signal was much weaker.
(G–J) Immunostaining on P10 cochlea (G, H) and vestibule (I, J) sagital sections via the LOXHD1 antibody (red) revealed expression in stereociliary bundles but not the cell body of hair cells. Nuclei were visualized with DAPI (blue) and F-actin with phalloidin (green).
(K) Immunogold localization of LOXHD1 in OHCs at P70. LOXHD1 was distributed along the length of stereocilia but was largely absent from their tips.
Scale bars represent 5 μm in (A)–(F), (H), (J); 100 μm in (G) and (I); and 100 nm in (K).

which maps to chromosome 18q12-q21 (LOD = 3.2), in a five-generation consanguineous Iranian family (Figure 6A). According to the NCBI Map Viewer (Human Genome Build 36.3), the interval contains 125 genes. The initial linkage analysis was based on three affected individuals (individuals V:4, V:5, and V:9 in Figure S8). The 1-LOD-drop region spanned 21 cM and contained 38 SNP markers, flanked by markers A-1691598 (rs1518148) and A-1642789 (rs619825) at chromosomal position 18q12-q21 (38–56 Mb) (Figure 6B; Figure S6). Individuals IV:2 and V:7 had their phenotypic status reviewed and changed after re-examination after the linkage analysis results showed homozygosity by state in individuals IV:2 and V:7. An additional linkage analysis with all five affected individuals and an estimated inbreeding loop above individual IV:2 produced a LOD score of 3.9 with an identical critical interval (data not shown). There were no other regions in the genome where the LOD score exceeded 3.

Based on the original analysis, all affected individuals were either homozygous by descent (HBD) or homozygous by state (HBS). Homozygosity by state was the result of the additional inbreeding loop from which individual IV:2 originated, which was not included in the pedigree for mapping. The green haplotype in Figure S8 is also HBD, being inherited through the unincorporated inbreeding loop. The DFNB77 interval includes *LOXHD1*, so we sequenced its 43 exons, identifying a homozygous stop mutation, c.2008C>T (p.R670X), in exon 15 in all affected family members tested (Figures 6A and 6C; Figure S2; Table S2). This exon was present in one of three human *LOXHD1* isoforms reported in GenBank (AK127869; Figure S2). The genotyped unaffected individuals (IV:1, V:1, V:6, and V:8) were carriers of the mutation (samples were unavailable for individuals V:2 and V:3) and of note, V:1 and V:6 had normal hearing at 42 and 38 years of age, respectively, consistent with ARNSHL (Figure 6E). The mutation was not found in 243 controls (486 chromosomes; 179 Centre d'Etudes du Polymorphisme Humain [CEPH] controls and 64 Iranian controls). The affected amino acid, R670, is located at the C-terminal end of the fifth PLAT domain and is conserved between human and mouse. Its substitution for a stop codon could lead to either a severely truncated protein or absence of the LOXHD1 protein secondary to nonsense-mediated decay (NMD) (Figure 6D).

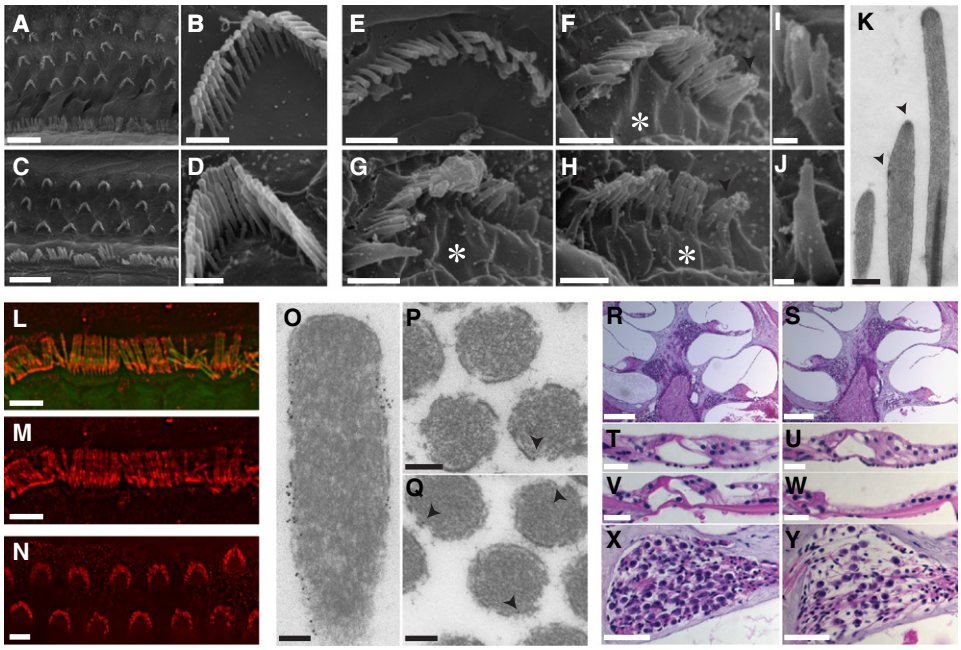

Figure 5. Hair Cell Morphology and Degeneration in *samba* Mice

(A–J) Analysis of the cochlea of 3-week-old wild-type and mutant animals by scanning electron microscopy.

(A and C) Three rows of OHCs and one row of IHCs are present in wild-type (A) and mutant (C) animals. The medial cochlear turn is shown.

(B and D) Hair bundles from OHCs in the medial part of the cochlea at higher magnification. The characteristic stereociliary staircase was present in hair cells from wild-types (B) and mutants (D).

(E–J) Stereociliary bundles from IHCs in the basal part of the cochlea in wild-type (E) and mutants (G–J). Note the ruffled apical hair cell surface (asterisks) and the fused stereocilia.

(K) The ultrastructure of stereocilia in P60 homozygous *samba* mice was analyzed by transmission electron microscopy (TEM); the characteristic electron-dense plaques at the tips of stereocilia and at the upper insertion site of the tip link (indicated by arrowheads) were present.

(L–N) LOXHD1 expression in homozygous *samba* mice was determined by immunofluorescence microscopy. LOXHD1 (red) was expressed in hair bundles of IHCs (L, M) and OHCs (N). In (L), samples were costained with phalloidin (green).

(O–Q) Immunogold localization of LOXHD1 in OHCs from homozygous *samba* mice (O, Q) or wild-types (P) at P60. The arrowheads point to the gold beads.

(R–Y) Histological sections through the cochlea of 3-month-old wild-type (R, T, V, X) and mutants (S, U, W, Y) were stained with hematoxylin and eosin. Degenerative changes were observed in the basal part of the cochlea (compare wild-type [V] and mutant [W]) but not in the apical region (compare wild-type [T] and mutant [U]). Spiral ganglion neurons were also degenerating (compare wild-type [X] and mutant [Y]).

Scale bars represent 10 μm in (A) and (C); 1 μm in (B), (D)–(H); 0.25 μm in (I) and (J); 250 nm in (K); 5 μm in (L)–(N); 100 nm in (O)–(Q); 200 μm in (R) and (S); 20 μm (T)–(W); and 50 μm in (X) and (Y).

Affected members of this family present a unique ARNSHL audioprofile, with preserved low-frequency hearing and a trend toward mild-to-moderate mid- (500–2000 Hz) and high- (>2000 Hz) frequency loss during childhood and adolescence (V:4, V:5; Figure 6E). The onset of hearing loss was self-reported by 7–8 years of age and progresses to become moderate-to-severe at mid and high frequencies during adulthood (V:9; Figure 6E), with flattening of the audiogram over time. All affected individuals reported age-appropriate developmental motor milestones for sitting and walking and remained free of tinnitus, balance disorders, or vertigo, consistent with normal vestibular function.

Discussion

We describe here the identification of the gene encoding LOXHD1, an evolutionarily highly conserved protein predicted to consist of 15 PLAT domains. Although single PLAT domains have been found in other proteins,[15] LOXHD1 is the first protein to be identified that consists entirely of PLAT domains. It is expressed in functionally mature mechanosensory hair cells, where it localizes along the length of the stereociliary membrane. Homozygous mutations in the human and mouse genes for LOXHD1 lead to auditory defects, indicating that the protein is essential for normal hair cell function. Consistent with this model, DPOAE recordings demonstrated functional defects in OHCs of *samba* mice. We found that a homozygous missense mutation in *Loxhd1* in *samba* mice causes profound deafness shortly after birth but that a homozygous nonsense mutation in DFNB77 patients causes progressive hearing loss, indicating that different mutations of LOXHD1 lead to distinct auditory phenotypes.

The PLAT domain was originally identified as an evolutionarily conserved protein domain in polycystin-1 and

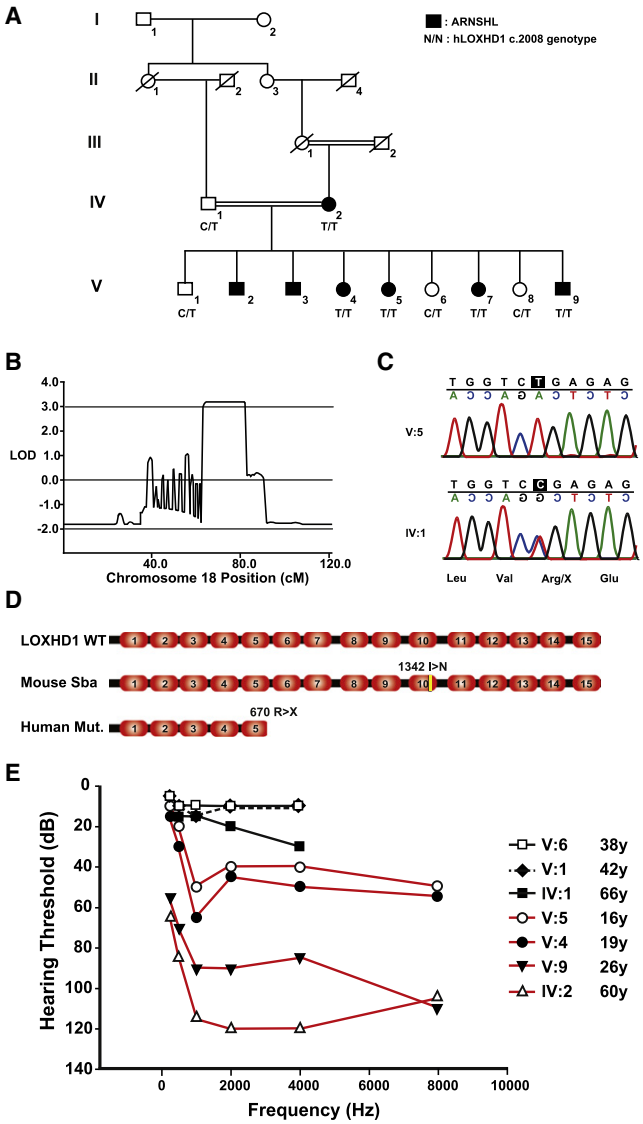

Figure 6. Mapping of the DFNB77 Mutation and Audiological Evaluation of Affected Patients

(A) Pedigree of the Iranian family. The c.2008 genotype is shown for those individuals included in the linkage analysis. DNA was unavailable from individuals V:2 and V:3. Open symbols unaffected; filled black symbols affected; double line consanguineous event; horizontal line deceased.

(B) Parametric LOD scores on chromosome 18. A genome-wide significant LOD score of 3.2 was identified for a region of approximately 21 cM on the q arm of chromosome 18.

(C) The c.2008C>T stop mutation in homozygous state in affected individual V:5 and heterozygous state in unaffected carrier IV:1.

(D) The p.R670X stop mutation is located at the end of the 5th PLAT domain of the LOXHD1 protein whereas the murine 1342I>N missense mutation is located in the 10th PLAT domain.

(E) Audiograms of representative affected family members. The audioprofile has a characteristic pattern with a general trend of initial mild-to-moderate mid (500–2000 Hz) and high (>2000 Hz) frequency loss during childhood and adolescence with preservation at low frequencies (V:4, V:5). The hearing loss progresses to be moderate-to-severe at mid and high frequencies during adulthood and flattens out over time (V:9).

its relatives.[15] PLAT domains have since been identified in other eukaryotic proteins such as lipoxygenases, the Rab6-interacting protein 1, triacylglycerol lipase, and lipoprotein lipase[17–20] and are likely an ancient structural motif as they are also present in the bacterial α-toxin of gas gangrene, and even in the gametocyte protein of *Plasmodium falciparum*.[14,21] LOXHD1 is unique, however, as the only known protein containing more than one PLAT domain—in fact, LOXHD1 consists only of PLAT domains. Highly conserved orthologs of *LOXHD1* are found in Chordates, which contain mechanosensory cells with protrusions rich in both F-actin and microtubules, but are absent in Ecdysozoa, with mechanosensors based solely on microtubules.[14,17,18,20] LOXHD1 therefore may have evolved with the development of F-actin-based mechanosensory organelles. Notably, developing cochlear hair cells contain at their apical surface in addition to the stereocilia a single kinocilium, which degenerates once the stereocilia have matured. LOXHD1 expression became prominent around the time of loss of the kinocilium and the protein might help to stabilize the stereociliary bundle in the absence of the kinocilium. Notably, vestibular hair cells, which do not shed their kinocilium, expressed reduced amounts of LOXHD1 and were not affected by the mutation.

Mutations in PLAT-domain-encoding genes are a common cause of human disease. For example, mutations in the genes for polycystin-1 and lipoprotein lipase led to polycystic kidney disease (PKD [MIM 601313]) and lipoprotein lipase deficiency (LPL [MIM 609708]), respectively.[22,23] Although the function of PLAT domains has not been elucidated, they are proposed to target proteins to the plasma membrane and in some cases to mediate protein-protein interactions.[15,16,24] The expression of LOXHD1 along the plasma membrane of stereocilia suggests that LOXHD1 may couple the plasma membrane to the underlying F-actin cytoskeleton, but other functions for LOXHD1 cannot be excluded. Interestingly, we observed defects in the morphology of stereocilia prior to hair cell degeneration. These changes were first apparent in *samba* mice in cochlear hair cells in the basal cochlear turn, which respond to the highest frequencies, and recapitulate the human phenotype in which auditory function in the medium-to-high frequency range is first affected.

Analysis by X-ray crystallography shows that a PLAT domain forms a β sandwich consisting of two sheets, each of four strands.[14,17,18,20] This structure resembles eukaryotic Ca^{2+}-binding C2 domains, although residues important for Ca^{2+} binding are not conserved in PLAT domains. It is interesting to note that some of the C2 domains are capable of Ca^{2+}-dependent membrane binding.[25] The difference in the auditory phenotypes in *samba* mice and human DFNB77 patients may be due to the distinct effects of the associated mutations on the structure of LOXHD1. The *samba* mutation, which affects PLAT domain 10, converts an isoleucine at position 1342 into an asparagine, destabilizing the β-sandwich structure with consequent predicted misfolding of a PLAT domain in the center of the LOXHD1 protein.

In DFNB77 patients, in contrast, the premature stop codon at the C-terminal end of the fifth PLAT domain could lead to a mutant protein that lacks the terminal 10 PLAT domains. The functional consequences of this normal-but-shortened protein may be a less severe phenotype than the phenotype associated with severe protein misfolding secondary to a missense mutation. Alternatively, the premature stop codon could lead to nonsense-mediated decay (NMD) and complete absence of LOXHD1 protein in hair cells.

To date, 77 ARNSHL genetic loci have been identified and 28 of the causally related genes have been cloned. Mutations in only three—*LOXHD1*, *MYO3A*, and *PJVK*—cause progressive ARNSHL (Table S3).[10,13] The fact that distinct LOXDH1 alleles lead to different auditory phenotypes in mice and humans may reflect species-specific effects of perturbation of the LOXHD1 protein in the inner ear. However, it is not unreasonable to expect that phenotypic variability may also be seen as with allele variants of other genes associated with ARNSHL. Lastly, it is noteworthy that transcripts encoding LOXHD1, MYO3A, and PJVK localize to hair cells, suggesting that defects in hair cell function are a common cause of progressive ARNSHL.

Supplemental Data

Supplemental Data include eight figures and three tables and can be found with this article online at http://www.ajhg.org/.

Acknowledgments

The authors sincerely thank the family for their participation in this study. They would also like to thank D. McCarthy for help with data assembly and K. Crozat and D. Logan for sharing expertise in fine mapping and bioinformatics. This research was funded by NIDCD grants DC007704, DC005965 (U.M.), and DC002842 (R.J.H.S.), the Skaggs Institute for Chemical Biology (U.M.), a fellowship from the Bruce Ford and Anne Smith Bundy Foundation (N.G.), an Australian National Health and Medical Research Council (NHMRC) Career Development Award (M.B.), and an NHMRC Overseas Biomedical Fellowship (M.S.H.). R.J.H.S. is the Sterba Hearing Research Professor, University of Iowa College of Medicine.

Received: May 6, 2009
Revised: July 22, 2009
Accepted: July 27, 2009
Published online: September 3, 2009

Web Resources

The URLs for data presented herein are as follows:

The Hereditary Hearing Loss Homepage, http://webh01.ua.ac.be/hhh/
NCBI Map Viewer, http://www.ncbi.nlm.nih.gov/mapview/
Online Mendelian Inheritance in Man (OMIM), http://www.ncbi.nlm.nih.gov/Omim/
UCSC genome browser, http://genome.ucsc.edu/

Accession Numbers

Accession number in GenBank of mouse *Loxhd1* cDNA is FJ50876.

References

1. Hildebrand, M.S., Newton, S.S., Gubbels, S.P., Sheffield, A.M., Kochhar, A., de Silva, M.G., Dahl, H.H., Rose, S.D., Behlke, M.A., and Smith, R.J. (2008). Advances in molecular and cellular therapies for hearing loss. Mol. Ther. *16*, 224–236.
2. Hilgert, N., Smith, R.J., and Van Camp, G. (2009). Function and expression pattern of nonsyndromic deafness genes. Curr. Mol. Med. *9*, 546–564.
3. Noben-Trauth, K., and Johnson, K.R. (2009). Inheritance patterns of progressive hearing loss in laboratory strains of mice. Brain Res. *1277*, 42–51.
4. Eyken, V., Van Camp, G., and Van Laer, L. (2007). The complexity of age-related hearing impairment: contributing environmental and genetic factors. Audiol. Neurootol. *12*, 345–358.
5. Friedman, L.M., Dror, A.A., and Avraham, K.B. (2007). Mouse models to study inner ear development and hereditary hearing loss. Int. J. Dev. Biol. *51*, 609–631.
6. Friedman, T.B., and Griffith, A.J. (2003). Human nonsyndromic sensorineural deafness. Annu. Rev. Genomics Hum. Genet. *4*, 341–402.
7. Frolenkov, G.I., Belyantseva, I.A., Friedman, T.B., and Griffith, A.J. (2004). Genetic insights into the morphogenesis of inner ear hair cells. Nat. Rev. Genet. *5*, 489–498.
8. Leibovici, M., Safieddine, S., and Petit, C. (2008). Mouse models for human hereditary deafness. Curr. Top. Dev. Biol. *84*, 385–429.
9. Vrijens, K., Van Laer, L., and Van Camp, G. (2008). Human hereditary hearing impairment: Mouse models can help to solve the puzzle. Hum. Genet. *124*, 325–348.
10. Schwander, M., Sczaniecka, A., Grillet, N., Bailey, J.S., Avenarius, M., Najmabadi, H., Steffy, B.M., Federe, G.C., Lagler, E.A., Banan, R., et al. (2007). A forward genetics screen in mice identifies recessive deafness traits and reveals that pejvakin is essential for outer hair cell function. J. Neurosci. *27*, 2163–2175.
11. Schwander, M., Xiong, W., Tokita, J., Lelli, A., Elledge, H.M., Kazmierczak, P., Sczaniecka, A., Kolatkar, A., Wiltshire, T., Kuhn, P., et al. (2009). A mouse model for nonsyndromic deafness (DFNB12) links hearing loss to defects in tip links of mechanosensory hair cells. Proc. Natl. Acad. Sci. USA *106*, 5252–5257.
12. Schneider, M.E., Dose, A.C., Salles, F.T., Chang, W., Erickson, F.L., Burnside, B., and Kachar, B. (2006). A new compartment at stereocilia tips defined by spatial and temporal patterns of myosin IIIa expression. J. Neurosci. *26*, 10243–10252.
13. Walsh, T., Walsh, V., Vreugde, S., Hertzano, R., Shahin, H., Haika, S., Lee, M.K., Kanaan, M., King, M.C., and Avraham, K.B. (2002). From flies' eyes to our ears: mutations in a human class III myosin cause progressive nonsyndromic hearing loss DFNB30. Proc. Natl. Acad. Sci. USA *99*, 7518–7523.
14. Naylor, C.E., Eaton, J.T., Howells, A., Justin, N., Moss, D.S., Titball, R.W., and Basak, A.K. (1998). Structure of the key toxin in gas gangrene. Nat. Struct. Biol. *5*, 738–746.
15. Bateman, A., and Sandford, R. (1999). The PLAT domain: A new piece in the PKD1 puzzle. Curr. Biol. *9*, R588–R590.
16. Aleem, A.M., Jankun, J., Dignam, J.D., Walther, M., Kuhn, H., Svergun, D.I., and Skrzypczak-Jankun, E. (2008). Human

platelet 12-lipoxygenase, new findings about its activity, membrane binding and low-resolution structure. J. Mol. Biol. *376*, 193–209.
17. Gillmor, S.A., Villasenor, A., Fletterick, R., Sigal, E., and Browner, M.F. (1997). The structure of mammalian 15-lipoxygenase reveals similarity to the lipases and the determinants of substrate specificity. Nat. Struct. Biol. *4*, 1003–1009.
18. Minor, W., Steczko, J., Stec, B., Otwinowski, Z., Bolin, J.T., Walter, R., and Axelrod, B. (1996). Crystal structure of soybean lipoxygenase L-1 at 1.4 A resolution. Biochemistry *35*, 10687–10701.
19. Recacha, R., Boulet, A., Jollivet, F., Monier, S., Houdusse, A., Goud, B., and Khan, A.R. (2009). Structural basis for recruitment of Rab6-interacting protein 1 to Golgi via a RUN domain. Structure *17*, 21–30.
20. van Tilbeurgh, H., Egloff, M.P., Martinez, C., Rugani, N., Verger, R., and Cambillau, C. (1993). Interfacial activation of the lipase-procolipase complex by mixed micelles revealed by X-ray crystallography. Nature *362*, 814–820.
21. Delrieu, I., Waller, C.C., Mota, M.M., Grainger, M., Langhorne, J., and Holder, A.A. (2002). PSLAP, a protein with multiple adhesive motifs, is expressed in Plasmodium falciparum gametocytes. Mol. Biochem. Parasitol. *121*, 11–20.
22. Harris, P.C., and Torres, V.E. (2008). Polycystic Kidney Disease. Annu. Rev. Med. *60*, 321–337.
23. Hegele, R.A., Tu, L., and Connelly, P.W. (1992). Human hepatic lipase mutations and polymorphisms. Hum. Mutat. *1*, 320–324.
24. Hu, J., and Barr, M.M. (2005). ATP-2 interacts with the PLAT domain of LOV-1 and is involved in Caenorhabditis elegans polycystin signaling. Mol. Biol. Cell *16*, 458–469.
25. Lemmon, M.A. (2008). Membrane recognition by phospholipid-binding domains. Nat. Rev. *9*, 99–111.
26. Senften, M., Schwander, M., Kazmierczak, P., Lillo, C., Shin, J.B., Hasson, T., Geleoc, G.S., Gillespie, P.G., Williams, D., Holt, J.R., et al. (2006). Physical and functional interaction between protocadherin 15 and myosin VIIa in mechanosensory hair cells. J. Neurosci. *26*, 2060–2071.
27. Eswar, N., Webb, B., Marti-Renom, M.A., Madhusudhan, M.S., Eramian, D., Shen, M.Y., Pieper, U., and Sali, A. (2006). Comparative protein structure modeling using Modeller. In Current Protocols in Bioinformatics, A.D. Baxevanis, ed. (San Francisco, CA: John Wiley and Sons), pp. 5.6.
28. Larkin, M.A., Blackshields, G., Brown, N.P., Chenna, R., McGettigan, P.A., McWilliam, H., Valentin, F., Wallace, I.M., Wilm, A., Lopez, R., et al. (2007). Clustal W and Clustal X version 2.0. Bioinformatics *23*, 2947–2948.
29. Di, X., Matsuzaki, H., Webster, T.A., Hubbell, E., Liu, G., Dong, S., Bartell, D., Huang, J., Chiles, R., Yang, G., et al. (2005). Dynamic model based algorithms for screening and genotyping over 100 K SNPs on oligonucleotide microarrays. Bioinformatics *21*, 1958–1963.
30. Rabbee, N., and Speed, T.P. (2006). A genotype calling algorithm for affymetrix SNP arrays. Bioinformatics *22*, 7–12.
31. Wigginton, J.E., and Abecasis, G.R. (2005). PEDSTATS: Descriptive statistics, graphics and quality assessment for gene mapping data. Bioinformatics *21*, 3445–3447.
32. Abecasis, G.R., Cherny, S.S., Cookson, W.O., and Cardon, L.R. (2002). Merlin—rapid analysis of dense genetic maps using sparse gene flow trees. Nat. Genet. *30*, 97–101.
33. Frazer, K.A., Ballinger, D.G., Cox, D.R., Hinds, D.A., Stuve, L.L., Gibbs, R.A., Belmont, J.W., Boudreau, A., Hardenbol, P., Leal, S.M., et al. (2007). A second generation human haplotype map of over 3.1 million SNPs. Nature *449*, 851–861.
34. Thiele, H., and Nurnberg, P. (2005). HaploPainter: A tool for drawing pedigrees with complex haplotypes. Bioinformatics *21*, 1730–1732.